Nano Energy 63 (2019) 103844

Contents lists available at ScienceDirect

Nano Energy

journal homepage: www.elsevier.com/locate/nanoen

Full paper

Direct muscle stimulation using diode-amplified triboelectric nanogenerators (TENGs)

Hao Wang[a,c,e], Jiahui Wang[a,b,c,e], Tianyiyi He[a,c,e], Zhou Li[f,**], Chengkuo Lee[a,b,c,d,e,*]

[a] Department of Electrical and Computer Engineering, National University of Singapore, Singapore, 117583, Singapore
[b] Singapore Institute for Neurotechnology (SINAPSE), National University of Singapore, Singapore, 117456, Singapore
[c] Center for Intelligent Sensor and MEMS, National University of Singapore, Singapore, 117581, Singapore
[d] NUS Graduate School for Integrative Sciences and Engineering, National University of Singapore, Singapore, 117456, Singapore
[e] Hybrid Integrated Flexible Electronic Systems, National University of Singapore, Singapore, 117583, Singapore
[f] CAS Center for Excellence in Nanoscience, Beijing Institute of Nanoenergy and Nanosystems, Chinese Academy of Sciences, National Center for Nanoscience and Technology (NCNST), Beijing, 100083, China

ARTICLE INFO

Keywords:
Diode-amplified TENG
Direct muscle stimulation
Self-powered
Output amplification
Resonance frequency of neuron
Exponential current waveform

ABSTRACT

Triboelectric nanogenerators (TENGs) device is proven to be a feasible method for self-powered direct neural/muscle stimulations. However, the higher threshold current required for direct muscle stimulation makes the efficiency of TENGs stimulator questionable. In this study, a new general configuration of TENG device, Diode amplified Triboelectric nanogenerators (D-TENGs), is proposed to greatly enhance the efficiency of direct muscle stimulation in three aspects: 1. the current can be much amplified by D-TENGs; 2. the exponential current pulse of D-TENGs device is the optimal waveform with the highest efficiency for muscle stimulation; 3. the D-TENGs can boost up the frequency of the current pulse to match with the resonance frequency of motoneurons in muscle, which is around 500 Hz. Thus, D-TENGs can be considered as the optimal TENG device for direct muscle stimulations. Meanwhile, the best electrode shift phenomenon observed in the experiments is explained and a general guideline for neural interface design is proposed.

1. Introduction

Since firstly invented by Z. L. Wang et al. [1], triboelectric nanogenerators (TENGs) have shown superior capability on energy harvester [2–9] and have been applied for various kinds of self-powered sensors [10–14]. Owing to its easy and low cost fabrication and the development of soft and wearable electronics [15–17], wide range material selection for flexible and soft device configuration and versatile capability, TENGs has been widely applied for various kinds of biomedical applications, such as pacemaker [18], heartbeat sensor [19], direct electrical stimulations of central nerve system (CNS) [20,21] and peripheral nerve system (PNS) [22–24]. Among them, the electrical nerve stimulation is the most surprising one: an intense nerve stimulation is achieved when either the output current or charge generated by the TENG device [23,24] is much lower than the threshold predicted by the conventional strength-duration relationship [25]. Although a comprehensive theoretical explanation for this abnormally high efficiency cannot be achieved, it is reported that the exponential current waveform, which is the exactly the current waveform of TENG device, may be the most effective for nerve stimulations [26]. Thus, TENG devices are very promising to be used as a standalone self-powered nerve stimulator in the future.

With the pioneer exploration of the direct nerve stimulation by TENGs, it is worthy of investigating whether the same scenario can be applied for direct muscle stimulations, which is an effective approach for the prevention or reversing of the muscle atrophy after losing the neural drive [27]. Meanwhile, functional electrical stimulation (FES) on muscle aims to recover meaningful movements to achieve complicated tasks of grasping and walking [27]. Moreover, electrical muscle stimulation is also proved to be an effective approach in the treatment of chronic venous insufficiency (CVI) of lower limbs [28–30], which is frequently caused by the failure of the calf muscle pump. The external muscle activations serving as musculovenous pumps [31] can supplement the blood circulation to avoid the CVI caused symptoms such as deep vein thrombosis (DVT) and venous ulcers. However, the challenge for direct muscle stimulation by TENGs is obvious. Different from the peripheral nerves or central nerves which are more spatially concentrated in a nerve bundle or a limited region, excitable motoneurons

* Corresponding author. Department of Electrical and Computer Engineering, National University of Singapore, Singapore, 117583, Singapore.
** Corresponding author.
E-mail addresses: zli@binn.cas.cn (Z. Li), elelc@nus.edu.sg (C. Lee).

https://doi.org/10.1016/j.nanoen.2019.06.040
Received 3 May 2019; Received in revised form 18 June 2019; Accepted 18 June 2019
Available online 22 June 2019
2211-2855/

in muscle tissues have a sparse spatial distribution. The threshold current required for activation of the muscle is very high, about hundreds of μA level, which is a great challenge for a TENG device with minimized dimension. Our previous study with extensive animal testing shows that with a palm-sized conventional TENGs, slight muscle stimulation can be achieved with an optimized electrode selection [32].

In this study, a new TENG device configuration, called Diode-amplified Triboelectric Nanogenerators (D-TENGs), is proposed to greatly amplify the triboelectric output for effective direct muscle stimulations. Different from the previous open-circuit voltage amplification by a high voltage diode [33], this D-TENGs is a general configuration which can easily be applied for many other TENG devices to significantly boost up the amplitude of current, power with a much reduced matched impedance. More importantly, D-TENGs can offer a unique property: it can boot up the frequency of the current waveform to match with the resonance frequency of the motoneurons, thus maximize the stimulation efficiency. Thus, the D-TENGs can be considered as the most effective device for direct muscle stimulation. Meanwhile, the best electrode pair (BEP) shift phenomenon observed in experiments is studied and explained. Based on this, some general guidelines for neural interface design is proposed.

2. Results

2.1. Working principle and characterization of D-TENGs

The structure and working process of the D-TENGs is shown in Fig. 1(a). It is a typical zig-zag shape stack-layer device with a confine to control the height of spacing [24]. There are 11 Al(Aluminium)-PTFE (Polytetrafluoroethylene) triboelectric surface pairs connected in parallel (All Al layers are connected together and all PTFE layers are connected together.). The dimension of each layer is 8 by 8 cm^2. An additional mechanical switch connected (Zener diode with 160 V breakdown voltage) is required to control a diode (Zener diode with 160 V breakdown voltage) connected in parallel (Fig. 1(b)), which is different from other reported TENGs. The detailed circuit connection is shown in Fig. 1(b). The similar switch operation has been demonstrated in previous studies [34–36]. This mechanical switch consists of two pieces of copper tapes and its configuration is shown in Fig. 1(a). Its operating logic is opposite to a normal switch, which is release-on and press-off. The detailed configuration of the device and the switch can be found in the Supplementary S1. The equivalent circuit of the whole setup including the D-TENGs, the diode, the switch and the load (neural interface and the muscle tissue) is shown in Fig. 1(b). The negative terminal of the diode is connected to the positive terminal of the D-TENGs, which is the Al surface. In one operation cycle, the switch will close once to short circuit the diode and thus, generate a high output of current pulse. Compared with a normal stack-layer TENGs which has synchronization issue, the charge generated by all layers of D-TENGs can be accumulated in front of the diode and transferred together within a shorter duration to achieve a short and high current pulse, as illustrated in Fig. 1(c). This amplified current pulse is sufficient and effective for direct muscle stimulation through a neural interface implanted in the muscle, as shown in Fig. 1(d). Thus, a muscle activation can be easily achieved with a standalone self-powered D-TENGs stimulator.

The detailed working mechanism of the D-TENGs for current amplification can be found in Fig. 2(a). At the initial state (Fig. 2(a–i)), the two contact surfaces are separated and the switch is on. The negative electrostatic charges on the PTFE surface are balanced by the positive charges on the top and bottom Al electrodes. Since the top Al electrode is closer to the PTFE film, the quantity of positive charges on the top Al electrode is higher than that of the bottom Al electrode. Then press the D-TENGs to turn off the switch (Fig. 2(a-ii)). Since the spacing between the top and bottom layer is reduced, the negative charges on the PTFE layer tend to be more balanced by the bottom Al electrode. A current pulse of pressing (Fig. 2(b)) is generated in this step. A further pressing to make the top and bottom surfaces fully contact (Fig. 2(a-ii)) to finish the current of pressing. Then release the D-TENGs to separate two contact surfaces (Fig. 2(a-iv)). The negative charges tend to be more balanced by the top Al electrode, thus a reverse current from the bottom to top should happen. However, these charges will be blocked by the diode until the D-TENGs is fully recovered to turn on the switch (Fig. 2(a–v)). The accumulated charges can be released immediately when the switch is on, generating a current of releasing as shown in Fig. 2(b). Compared with the output of the current of other reported TENGs, this releasing current can be much more amplified. A detailed comparison of the current pulses for the device with and without the diode amplification is shown in Fig. 2(c). Due to the too low releasing current for the cases without diode, as seen in Fig. 2(b), the pressing current is used instead. For the cases with diode, we still use the releasing current. Meanwhile, to mimic the practical condition in muscle stimulation, which can be seen in Fig. 3, the experiment is conducted by hand tapping with almost the same tapping force. The measured

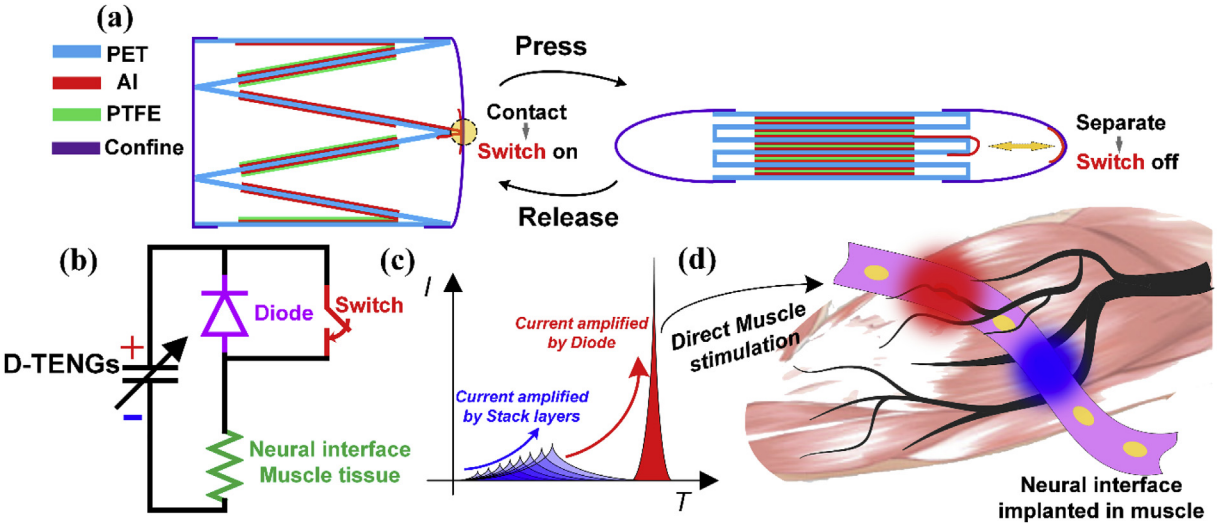

Fig. 1. D-TENGs for direct muscle stimulation. (a). Detailed structure and operation process of the D-TENGs; (b) The equivalent circuit of the D-TENGs for muscle stimulations; (c) The current pulses amplified by the diode; (d) The current amplified by the diode can directly stimulate the muscle with an implanted neural interface within the muscle.

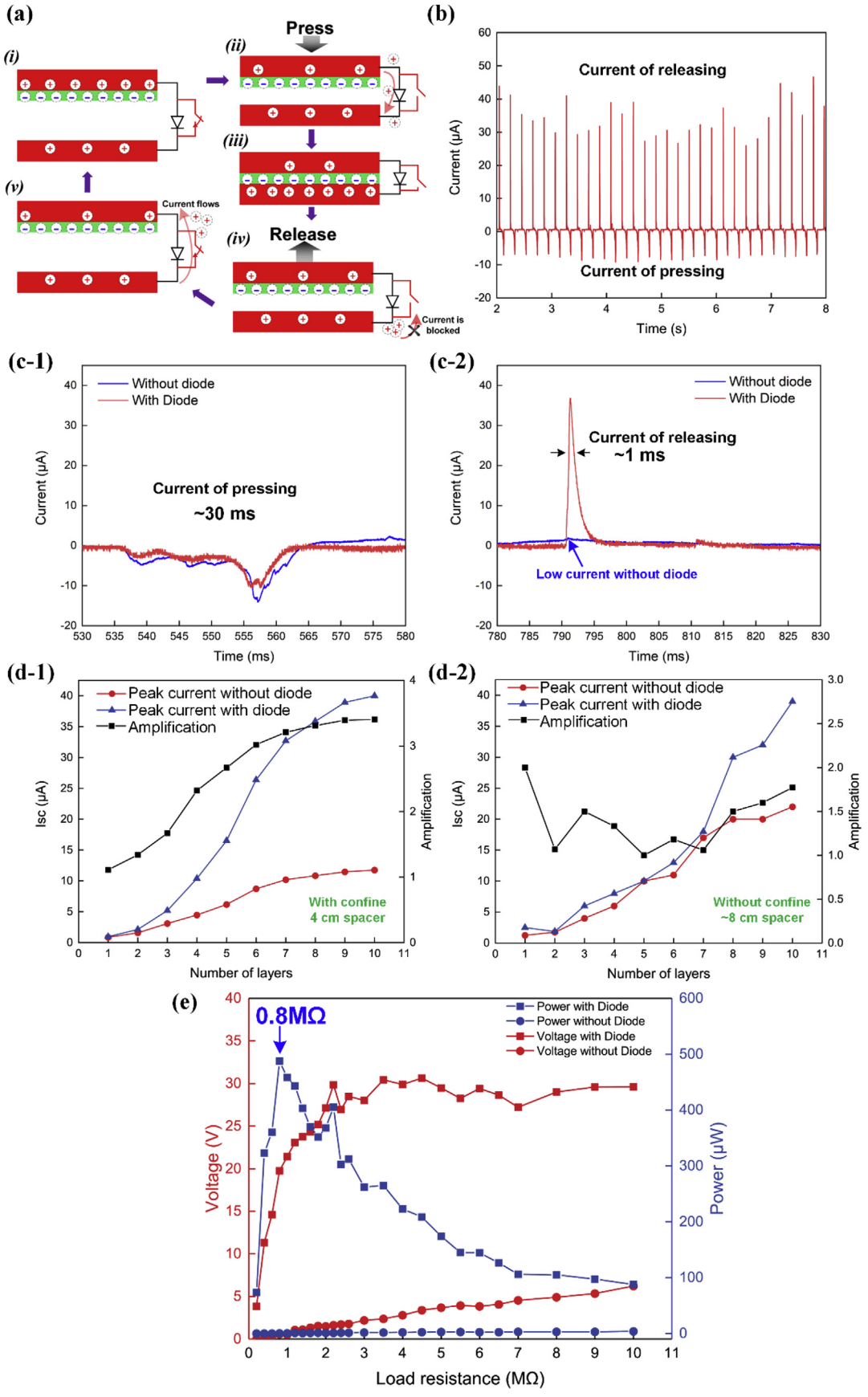

(caption on next page)

Fig. 2. Characterization of D-TENGs: (a) The working principle of the D-TENGs for current amplification; (b) A typical current profile of the D-TENGs; (c-1) The comparison of the pressing current peaks with and without the diode amplification; (c-2) The comparison of the releasing current peaks with and without the diode amplification; (d-1) amplification of the short circuit current (I_{sc}) with a spacer confine (Pressing current for without diode and releasing current for with diode); (d-2) amplification of the I_{sc} without a spacer confine (Pressing current for without diode and releasing current for with diode); (e) the output voltage and power with different load resistance with and without the diode amplification.

maximum impact force for the tapping is 40–50 N and the exact tapping procedure can be found in Supplementary video. For the current of pressing (Figs. 2(c-1)), there is almost no difference between the two current pulses, since the diode has no effect during the pressing. This current of pressing lasts about 30 ms as long as the whole pressing process in this case. The situation for the current of releasing without diode amplification is the same as other stack-layer TENGs. The current of releasing also lasts the whole releasing process, which is a spontaneous procedure slower than the pressing. Thus, the current pulse is even longer with a much-reduced amplitude shown in Fig. 2(c-2). However, for the case with diode amplification, the charge can be accumulated by the diode and released instantaneously when the switch is on. All the current flow is compressed into a very short duration, about 1 ms for this device, to boost up the amplitude while the quantity of charges remains the same.

Supplementary video related to this article can be found at https://doi.org/10.1016/j.nanoen.2019.06.040.

It is observed that the effect of the height of the spacer on the current output of the D-TENGs tends to diminish by increasing the height. The detailed explanation can be found in Supplementary S3. In some case, a lower spacer can even achieve a higher output, which is opposite to the reported TENGs. Normally, TENGs require a higher spacer for higher and more stable output. Here we make a comparison between two cases: 4 cm spacer with a confine, ~8 cm spacer without a confine. The detailed data is shown in Fig. 2(d) by changing the number of stack-layers. The short circuit currents for the device with and without the diode amplification are recorded to calculate how many times the current is amplified. It is noted that for the case without diode amplification, a higher spacer can achieve a higher current (20 μA of 8 cm spacer is higher than 10 μA of 4 cm spacer with 11 layers). This is reasonable for the other reported TENGs. But for the case with diode amplification, the maximum currents for 11 layers are the same with the different height of spacer, ~40 μA. Thus, the case of 4 cm spacer can achieve a higher current amplification, which is 3.4 with 11 layers, while the case of ~8 cm spacer only achieves the current amplification of around 2.

With this current amplification, D-TENGs can also enhance the output power with a much reduced matched impedance. The detailed comparison is shown in Fig. 2(e). For the case without the diode, the output power peaks at 2.83 μW with around 6 MΩ matched impedance. With the diode amplification, the output power can be boosted up to 500 μW with a 0.8 MΩ matched impedance.

In summary, with an extra diode, the D-TENGs can greatly boost up the current and output power with a much reduced matched impedance. Meanwhile, the current pulse is much reduced, which is a frequency up-boost effect. Here the frequency refers to the reciprocal pf the signal pulse width than the period of the operation cycle. This frequency up-boost makes direct muscle stimulation more effective, which will be demonstrated in the following section. Moreover, the D-TENGs is more like a general configuration rather than an exact device, which can be applied to TENGs with other structures and materials. With a better material selection and surface treatment, the output can be further improved.

2.2. Results of direct muscle stimulation using D-TENGs

Fig. 3 shows the results of direct muscle stimulation using D-TENGs. The testing setup is shown in Figs. 3(a-1). A home-made polyimide neural interface developed (Figs. 3(a-2)) was implanted in the TA (Tibialis anterior) muscle to generate a forward kicking by electrical stimulation. The force is measured by the force gauge which is connected to the leg with a wire. The neural interface is connected to the D-TENGs to apply electrical stimulations. There are 6 electrode pads on the neural interface, allowing different electrode pair combinations for the stimulation (Figs. 3(a-2)). Since the stimulation result is highly affected by the current polarity and the relative position between the electrode pair and the target motoneuron, the force generated by the D-TENGs will be different by changing the electrode pair combinations. Thus, to make a complete investigation of the stimulation by D-TENGs, all possible combinations were studied and the results are shown with a matrix in Fig. 3(b–c). In our previous study, it was proved to be an effective method to characterize the efficiency difference between all possible electrode combinations [32]. In this matrix, each square represents a specific electrode pair combination. Since the polarity of the current pulse is also a parameter to be considered, we will differentiate the positive (connected to the Al layer) and negative (connected to the PTFE layer) electrodes. For example, (1,5) means pad 1 and 5 are connected to the positive and negative terminals of the D-TENGs, respectively. It is noted that combinations such as (1,1) and (2,2) are unavailable since one electrode pad cannot be connected to both the positive and negative terminals. The experiment details can be found in Supplementary S2.

We performed four tests to compare the stimulation efficiency of the device without and with the diode amplification, shown in Fig. 3(b) and (c), respectively. For the case of no diode amplification, there is no electrode pair to generate any force in test 1 and 2. It means that in these two tests, the implanted neural interface is too far away from the motoneurons. In test 3 and 4, only some specific pairs can generate very low force. The highest force recorded is 0.12 N as shown in Figs. 2(d-1). It can be seen that all the successful stimulations are related with some specific electrode pads, which is pad 1 in test 3 and pad 2 in test 4. This means that these two pads are very close to the target motoneuron. Since the current without diode amplification is very low, a successful stimulation can only happen when the electrodes are very close to the motoneuron. However, for the cases with the diode amplification, almost all the combinations can be used for stimulation with a much higher force generation. The highest forced recorded is 0.24 N shown in Figs. 3(d-2). The video showing the lag kicking by the D-TENGs stimulation can be found in Supplementary video.

3. Discussion

There are three interesting points to be observed. Firstly, it seems that the current pulses generated by the TENGs are more effective for muscle stimulation than commercialized stimulators. For most of the cases, the triboelectric device can achieve the same stimulation results with either a lower current or a lower charge quantity. Here we summarized all the stimulations results by current pulses generated by the D-TENGs and a commercial stimulator (A-M SYSTEMS model 4100) in Fig. 3(e). The data points for the triangle, square and sinewave current pulses are from Fig. 4 and Fig. 5 in the following sections. As seen, for the square the triangle current pulses, the working range is normally higher than 500 μA while the D-TENGs can achieve the same force at a much lower current range. In this case, the current is 10 μA and 40 μA for D-TENGs with and without the diode amplification, respectively, as characterized in Fig. 2(c). The same phenomenon happens in our previous study of sciatic nerve stimulation by TENGs [23,24]. In sciatic nerve stimulation, it was also observed that a strong stimulation can be

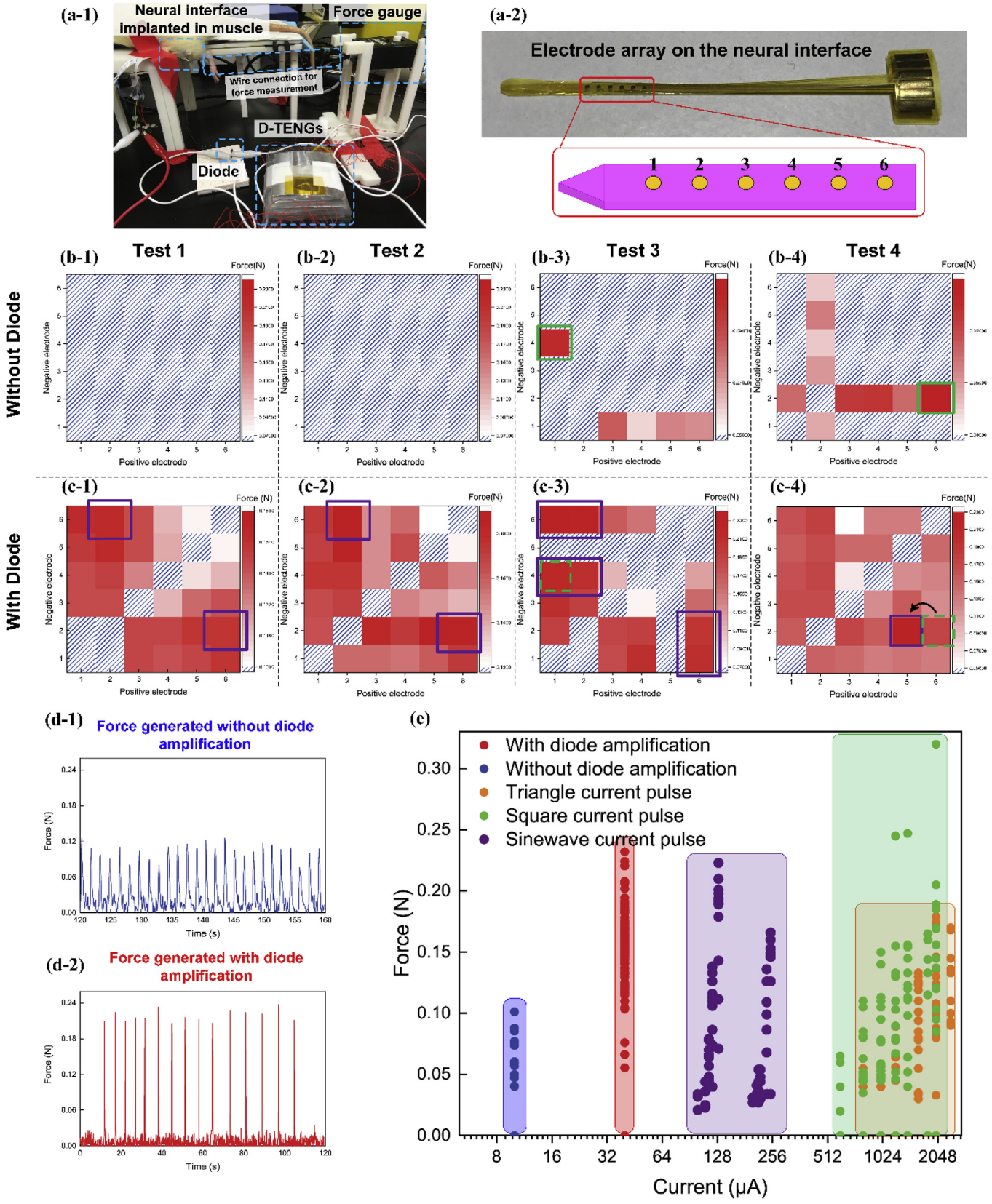

Fig. 3. (a) Test setup and experiment configuration of the direct muscle stimulation by D-TENGs; (b) the image of the neural interface with electrode pad array, which is numbered from 1 to 6, corresponding to the coordination of the matrix used in (b–c); (b–c) Four tests of the direct muscle stimulation by the D-TENGs with and without the diode amplification. Each block in the matric refers to the generated force with a specific electrode pair combination. For example, (1,5) means the pad 1 and 5 are connected to the positive and negative terminals of the D-TENGs, respectively. The combination of highest force generation is labeled with green and purple blocks for results with and without diode amplification, respectively; (d) The typical force generated by the D-TENGs with (d1) and without (d2) the diode amplification; (e) The summary of all the testing results by using D-TENGs and commercial stimulators with different current waveforms and amplitudes.

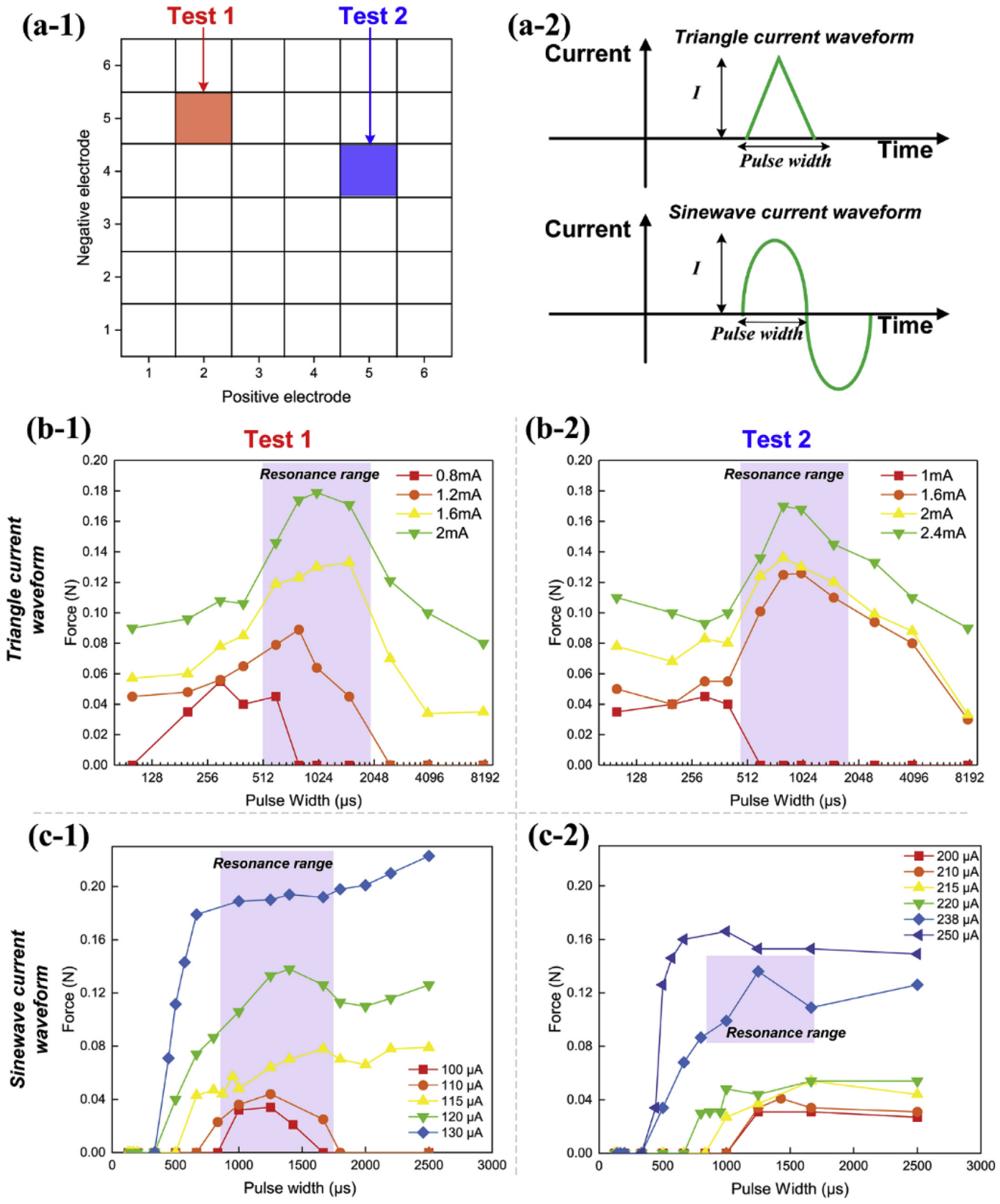

Fig. 4. Stimulation results showing the resonance frequency of the motoneuron in the TA muscle. (a) Testing configuration: two electrode pair combinations (a-1) are selected to apply the triangle pulse and sinewave pulse in (a-2) by changing the current amplitudes and pulse widths; (b) The force curve with different pulses width and current amplitudes of triangle current pulses, showing a maximum force at the pulse width of ~1000 μs, it is noted that the time axis is non-linear; (c) The force curve with different pulses width and current amplitudes of sinewave current pulses, showing a maximum force at the pulse width of ~1000 μs

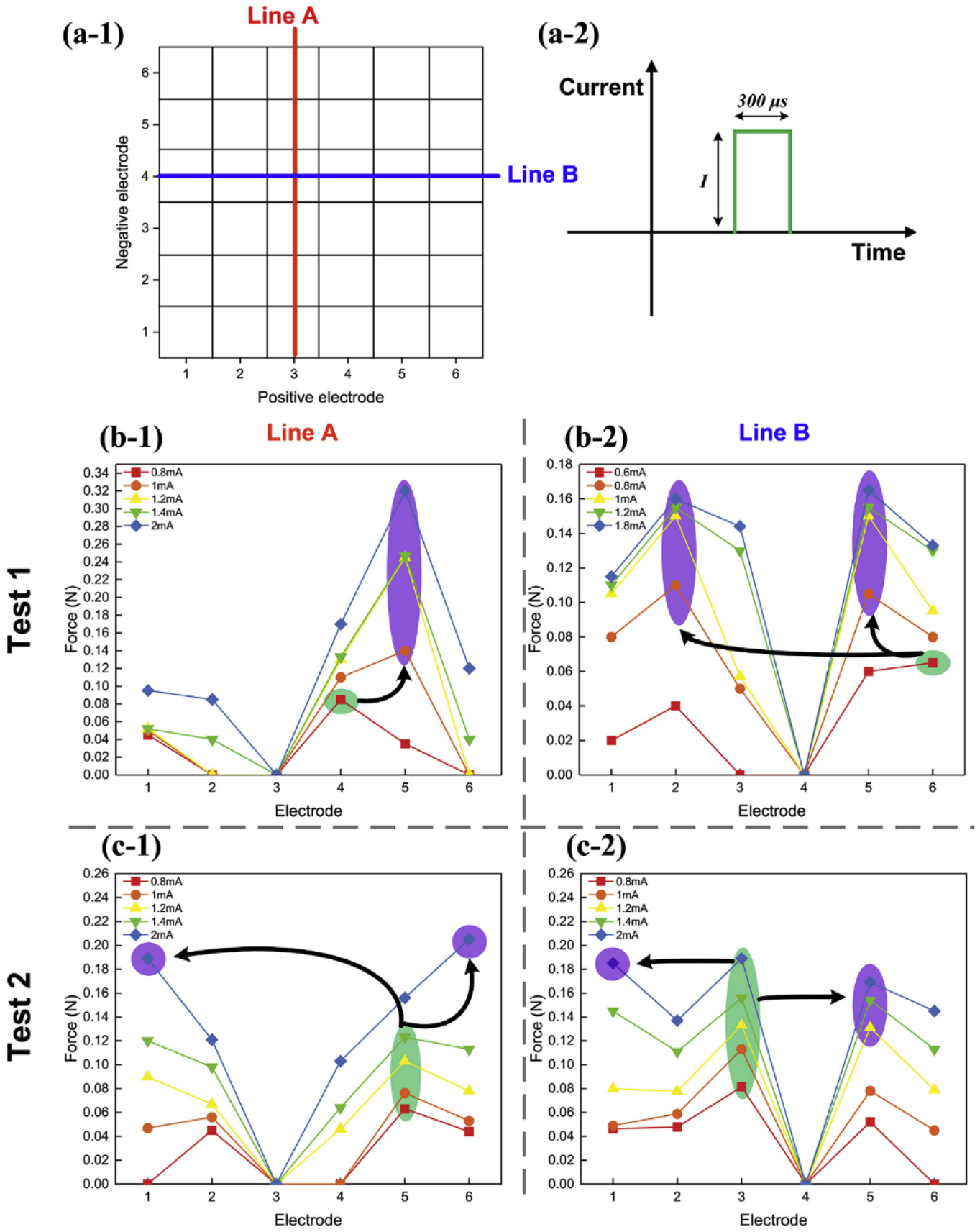

Fig. 5. The shift of the BEP (Best electrode pair) in stimulations with square current pulses. (a) Testing configuration: the electrode pairs along two lines, line A and line B, are selected to apply the 300 μs square current pulse in (a-2) by changing the current amplitude; (b) The results of test 1; (c) The results of test 2.

achieved with a very low current generated by the TENGs. One possible reason is that the exponential current waveform involved in the TENGs output is more effective than other shapes of waveforms for nerve stimulations. Some early studies have shown confirmatory results to support this possibility [26]. Our own investigation also shows supportive evidence [23]. However, making a totally fair comparison of the stimulation efficiency is quite difficult since we cannot assign equal charge, current and power for different waveforms simultaneously. Thus, it may be too early to claim that TENGs is the most effective device for nerve and muscle stimulations. But current results show that TENGs is very promising for nerve stimulations.

The second point is that the enhanced force generation by the diode amplification may not only come from the increased current amplitude but is also affected by the frequency up-boost effect. As shown in Fig. 2(c), the D-TENGs can achieve a very narrow current pulse, which accidently matches the resonance frequency of the target motoneuron. It was reported that the neuron can have a higher response to the current with a matched frequency [37–40]. To validate this point, we used the triangle current pulse, which resembles the current pulse of D-TENGs (shown in Fig. 2(c-2)) to measure the resonance frequency in the muscle stimulations. Two random electrode pairs are selected, as shown in Figs. 4(a-1), to apply the triangle current pulses and sinewave current pulses with different pulse widths and current amplitudes, as shown in Figs. 4(a-2). The reason for using the sinewave is that the sinewave is single frequency signal which is more suitable for validating the resonance frequency hypothesis. For the situation of the triangle waveform, both the testing results in Figs. 4(b-1) and (b-2) show the same trend: the force reaches the maximum at the pulse width of ~1000 μs, which is very close to the current pulse of D-TENGs as measured in Figs. 3(c-2). For the situation of the sinewave current, the testing results show a more complex trend. For test 1 in Figs. 4(c-1), the resonance effect is distinct when the current is low but gradually disappears by increasing the current amplitude. For another test in Figs. 4(c-2), only a small resonance peak is observed at medium current. For the case of both low and high current, the resonance peak is not well observed. Considering the unclear detailed mechanism of electrical nerve stimulation, we cannot fully explain the complex force curve observed in the sinewave test currently. However, the resonance effect at around 1000 μs pulse width is repeated observed in different tests with different current waveforms, it is strong evidence to support that the resonance frequency of the motoneuron in TA muscle is very close to 500 Hz (1000 μs for monophasic waveform). The up-boosted current frequency is also a part of the reason that accounts for the enhanced force generation. It also indicates that the D-TENGs is particular and much more suitable than other reported TENGs for direct muscle stimulation.

The third point is the best electrode pair (BEP) shift problem. It was observed that the BEP, which is the electrode pair to achieve the maximum force, can shift in the same test by increasing the current amplitude. The BEPs in each test are labeled by green and purple blocks in Fig. 3(b) and (c) for cases without and with the diode amplification, respectively. As seen, in test 3, the BEP is (1,4) without diode amplification (Fig. 3(b-3)). However, in the same test with diode amplification (Fig. 3(c-3)), there are 6 blocks with almost the same maximum force. Among them, (1,6), (2,6) and (2,4) have no force while (6,2) and (6,1) only generate a very low force without the diode. This phenomenon is more distinct in test 4 (Figs. 3(b-4) & (c-4)): the BEP shifts from (6,2) to (5,2).

To validate this phenomenon, we perform another test with commercial stimulator by applying square current pulses. The testing configuration is shown in Fig. 5(a). We randomly selected the electrode pairs along two lines, line A and line B, to apply the 300 μs square current pulse with different amplitudes. The test was repeated twice on two rats and the results are shown in Fig. 5(b–c). For line A, the positive electrode is fixed on pad 3 and the negative electrode changes from 1 to 6. For line B, the negative electrode is fixed on pad 4 and the positive electrode changes from 1 to 6. The BEPs before and after the shifting are labeled as green and purple circles, respectively, by increasing the current. As seen, with the same current increment, the force increment varies with different electrode pairs. Thus the BEP shift is a common phenomenon.

The phenomenon can be explained by involving the stimulation of multiple motoneuron branches in the test [41,42]. There are multiple neuron branches can be stimulated in the muscle. Consider there are two electrode pairs, pair A and B, to stimulate two neural branches, branch 1 and 2. Pair A is very close to branch 1 and quite far from branch 2. Pair B is between branch 1 and 2. Then pair A is very dedicated to the stimulation of branch 1. The stimulation strength of branch 1 can be very high even the current is low. However, pair B can stimulate both branch 1 and 2 but requires a relatively higher current. Then, as a result, the force of pair A will be higher than pair B at low current. But by increasing the current, pair B can gradually stimulate both branches and generate a higher force than pair A. The shift of BEP happens. This is just a simple case while the actual situation can be much more complicated. But we still can obtain some guidelines for the muscle stimulations by a stimulator with limited power output, which is the case for D-TENG. When the energy is limited, finding the BEP for best efficiency is very critical. Since the BEP shift is an inevitable issue, a force mapping like the matric used in Fig. 3 is a necessary effort to locate the BEP. Meanwhile, it also suggests that a neural interface with an electrode pad array is a good design for the optimization of muscle stimulation efficiency.

In conclusion, a Triboelectric nanogenerators (TENGs) device with a new configuration, called Diode amplified Triboelectric nanogenerators, is proven to be a feasible method for self-powered direct neural/muscle stimulations. It overcomes the higher threshold current obstacle for direct muscle stimulation, making TENGs as effective stimulators for neuroprosthesis. It greatly enhances the efficiency of direct muscle stimulation in three aspects: 1. the current can be much amplified by D-TENGs; 2. the exponential current pulse of D-TENGs device is the optimal waveform with the highest efficiency for muscle stimulation; 3. the D-TENGs can boost up the frequency of the current pulse to match with the resonance frequency of motoneurons in muscle, which is around 500 Hz. Meanwhile, the best electrode shift phenomenon observed in the experiments is explained and a general guideline for neural interface design is proposed.

4. Methods

4.1. Fabrication of the stack-layer D-TENGs

A long PET film with 9 cm width is folded to form the zig-zag structure. The dimension of each folded layer is 9 cm by 9 cm. Then the Al tapes with 8 cm by 8 cm dimension are attached to each folded layer to form the electrodes of D-TENGs. PTFE layers are attached on the Al tapes on odd layers to form the Al-PTFE contact surface pair. All the Al layers without PTFE coating are considered as positive terminals and are connected with wires. All the Al layers with PTFE coating are considered as negative terminals and are connected with wires. Thus, all triboelectric pairs are connected in parallel. An additional PTFE layer is wrapped around the device to form the confine. Two electrodes are attached as shown in Fig. S1 to form the mechanical switch to control the diode.

4.2. Tibialis anterior (TA) muscle test electrode configuration, experiment procedure and testing setup

Sprague-Dawley rats (around 450 g) were used in acute experiments. Rats were housed and cared for in compliance with the guidelines of the National Advisory Committee for Laboratory Animal Research (NACLAR) and were humanely euthanized after the experiment. During the experiment, isoflurane was used to induce and maintain general anesthesia (Aerrane®, Baxter Healthcare Corp., USA).

The Tibialis Anterior (TA) muscle was exposed for electrode implantation. Our home-made double-side polyimide electrode was sutured into the muscle belly, transversal to muscle fibers in TA muscle. Current stimulation was delivered from either A-M SYSTEMS model 4100 isolated high-power stimulator or the D-TENGs. Force was measured with a dual-range force sensor (Hand dynamometer, Vernier, USA with NI-DAQ USB-6008, National Instruments, USA) tied to the ankle of the animal.

Author contributions

Hao W. proposed the D-TENGs configuration and fabricated the device. Hao W. and Tianyiyi H. characterized the device output. Hao W. and Jiahui W. conducted the animal tests. Hao W. processed the data and proposed the experimental explanation. Prof. Zhou L. and Prof. Chengkuo L. provided general guidance and supervision of the project. Prof Zhou L. and Prof. Chengkuo L. reviewed and edited the manuscript. Authors declare no competing interests. All data is available in the main text or the supplementary materials.

Acknowledgments

This work was supported by grants from the National Research Foundation Competitive research programme (NRF-CRP) 'Peripheral Nerve Prostheses: A Paradigm Shift in Restoring Dexterous Limb Function' (NRF-CRP10-2012-01), National Research Foundation Competitive research programme (NRF-CRP) 'Energy Harvesting Solutions for Biosensors' (R-263-000-A27-281), National Research Foundation Competitive research programme (NRF-CRP) 'Piezoelectric Photonics Using CMOS Compatible AlN Technology for Enabling The Next Generation Photonics ICs and Nanosensors' (R-263-000-C24-281), Faculty Research Committee (FRC) 'Thermoelectric Power Generator (TEG) Based Self-Powered ECG Plaster - System Integration (Part 3)' (R-263-000-B56-112) and HIFES Seed Funding 'Hybrid Integration of Flexible Power Source and Pressure Sensors' (R-263-501-012-133), National Natural Science Foundation of China (No. 61875015, 31571006).

Appendix A. Supplementary data

Supplementary data to this article can be found online at https://doi.org/10.1016/j.nanoen.2019.06.040.

References

[1] F.-R. Fan, Z.-Q. Tian, Z. Lin Wang, Flexible triboelectric generator, Nano Energy 1 (2012) 328–334, https://doi.org/10.1016/J.NANOEN.2012.01.004.
[2] H. Ouyang, J. Tian, G. Sun, Y. Zou, Z. Liu, H. Li, L. Zhao, B. Shi, Y. Fan, Y. Fan, Z.L. Wang, Z. Li, Self-powered pulse sensor for antidiastole of cardiovascular disease, Adv. Mater. 29 (2017) 1703456, https://doi.org/10.1002/adma.201703456.
[3] S. Cheon, H. Kang, H. Kim, Y. Son, J.Y. Lee, H.-J. Shin, S.-W. Kim, J.H. Cho, High-Performance triboelectric nanogenerators based on electrospun polyvinylidene fluoride–silver nanowire composite nanofibers, Adv. Funct. Mater. 28 (2018) 1703778, https://doi.org/10.1002/adfm.201703778.
[4] X. Chen, Y. Wu, A. Yu, L. Xu, L. Zheng, Y. Liu, H. Li, Z. Lin Wang, Self-powered modulation of elastomeric optical grating by using triboelectric nanogenerator, Nano Energy 38 (2017) 91–100, https://doi.org/10.1016/J.NANOEN.2017.05.039.
[5] H.-J. Yoon, H. Ryu, S.-W. Kim, Sustainable powering triboelectric nanogenerators: approaches and the path towards efficient use, Nano Energy 51 (2018) 270–285, https://doi.org/10.1016/J.NANOEN.2018.06.075.
[6] Y. Chen, Y. Jie, J. Wang, J. Ma, X. Jia, W. Dou, X. Cao, Triboelectrification on natural rose petal for harvesting environmental mechanical energy, Nano Energy 50 (2018) 441–447, https://doi.org/10.1016/J.NANOEN.2018.05.021.
[7] X. Chen, X. Pu, T. Jiang, A. Yu, L. Xu, Z.L. Wang, Tunable optical modulator by coupling a triboelectric nanogenerator and a dielectric elastomer, Adv. Funct. Mater. 27 (2017) 1603788, https://doi.org/10.1002/adfm.201603788.
[8] R. Hinchet, A. Ghaffarinejad, Y. Lu, J.Y. Hasani, S.-W. Kim, P. Basset, Understanding and modeling of triboelectric-electret nanogenerator, Nano Energy 47 (2018) 401–409, https://doi.org/10.1016/J.NANOEN.2018.02.030.
[9] J. Chen, H. Guo, X. Pu, X. Wang, Y. Xi, C. Hu, Traditional weaving craft for one-piece self-charging power textile for wearable electronics, Nano Energy 50 (2018) 536–543, https://doi.org/10.1016/J.NANOEN.2018.06.009.
[10] L. Dhakar, S. Gudla, X. Shan, Z. Wang, F.E.H. Tay, C.-H. Heng, C. Lee, Large scale triboelectric nanogenerator and self-powered pressure sensor array using low cost roll-to-roll UV embossing, Sci. Rep. 6 (2016) 22253 https://doi.org/10.1038/srep22253.
[11] Q. Shi, H. Wu, H. Wang, H. Wu, C. Lee, Self-powered gyroscope ball using a triboelectric mechanism, Adv. Energy Mater. 7 (2017) 1701300, https://doi.org/10.1002/aenm.201701300.
[12] Q. Shi, H. Wang, T. Wang, C. Lee, Self-powered liquid triboelectric microfluidic sensor for pressure sensing and finger motion monitoring applications, Nano Energy 30 (2016) 450–459, https://doi.org/10.1016/J.NANOEN.2016.10.046.
[13] H. Wang, H. Wu, D. Hasan, T. He, Q. Shi, C. Lee, Self-powered dual-mode amenity sensor based on the water–air triboelectric nanogenerator, ACS Nano 11 (2017) 10337–10346, https://doi.org/10.1021/acsnano.7b05213.
[14] Z. Liu, Y. Ma, H. Ouyang, B. Shi, N. Li, D. Jiang, F. Xie, D. Qu, Y. Zou, Y. Huang, H. Li, C. Zhao, P. Tan, M. Yu, Y. Fan, H. Zhang, Z.L. Wang, Z. Li, Transcatheter self-powered ultrasensitive endocardial pressure sensor, Adv. Funct. Mater. 29 (2019) 1807560, https://doi.org/10.1002/adfm.201807560.
[15] J. Kim, M. Lee, H.J. Shim, R. Ghaffari, H.R. Cho, D. Son, Y.H. Jung, M. Soh, C. Choi, S. Jung, K. Chu, D. Jeon, S.-T. Lee, J.H. Kim, S.H. Choi, T. Hyeon, D.-H. Kim, Stretchable silicon nanoribbon electronics for skin prosthesis, Nat. Commun. 5 (2014) 5747 https://doi.org/10.1038/ncomms6747.
[16] C. Lim, Y. Shin, J. Jung, J.H. Kim, S. Lee, D.-H. Kim, Stretchable conductive nanocomposite based on alginate hydrogel and silver nanowires for wearable electronics, Apl. Mater. 7 (2018) 31502, https://doi.org/10.1063/1.5063657.
[17] J. Choi, A.J. Bandodkar, J.T. Reeder, T.R. Ray, A. Turnquist, S.B. Kim, N. Nyberg, A. Hourlier-Fargette, J.B. Model, A.J. Aranyosi, S. Xu, R. Ghaffari, J.A. Rogers, Soft, Skin-integrated multifunctional microfluidic systems for accurate colorimetric analysis of sweat biomarkers and temperature, ACS Sens. 4 (2019) 379–388, https://doi.org/10.1021/acssensors.8b01218.
[18] Q. Zheng, B. Shi, F. Fan, X. Wang, L. Yan, W. Yuan, S. Wang, H. Liu, Z. Li, Z.L. Wang, In vivo powering of pacemaker by breathing-driven implanted triboelectric nanogenerator, Adv. Mater. 26 (2014) 5851–5856, https://doi.org/10.1002/adma.201402064.
[19] Y. Ma, Q. Zheng, Y. Liu, B. Shi, X. Xue, W. Ji, Z. Liu, Y. Jin, Y. Zou, Z. An, W. Zhang, X. Wang, W. Jiang, Z. Xu, Z.L. Wang, Z. Li, H. Zhang, Self-powered, one-stop, and multifunctional implantable triboelectric active sensor for real-time biomedical monitoring, Nano Lett. 16 (2016) 6042–6051, https://doi.org/10.1021/acs.nanolett.6b01968.
[20] Y. Fu, M. Zhang, Y. Dai, H. Zeng, C. Sun, Y. Han, L. Xing, S. Wang, X. Xue, Y. Zhan, Y. Zhang, A self-powered brain multi-perception receptor for sensory-substitution application, Nano Energy 44 (2018) 43–52, https://doi.org/10.1016/J.NANOEN.2017.11.068.
[21] Y. Dai, Y. Fu, H. Zeng, L. Xing, Y. Zhang, Y. Zhan, X. Xue, A self-powered brain-linked vision electronic-skin based on triboelectric-photodetecing pixel-addressable matrix for visual-image recognition and behavior intervention, Adv. Funct. Mater. 28 (2018) 1800275, https://doi.org/10.1002/adfm.201800275.
[22] X.-S. Zhang, M.-D. Han, R.-X. Wang, B. Meng, F.-Y. Zhu, X.-M. Sun, W. Hu, W. Wang, Z.-H. Li, H.-X. Zhang, High-performance triboelectric nanogenerator with enhanced energy density based on single-step fluorocarbon plasma treatment, Nano Energy 4 (2014) 123–131, https://doi.org/10.1016/J.NANOEN.2013.12.016.
[23] S. Lee, H. Wang, J. Wang, Q. Shi, S.-C. Yen, N.V. Thakor, C. Lee, Battery-free neuromodulator for peripheral nerve direct stimulation, Nano Energy 50 (2018) 148–158, https://doi.org/10.1016/J.NANOEN.2018.04.004.
[24] S. Lee, H. Wang, Q. Shi, L. Dhakar, J. Wang, N.V. Thakor, S.-C. Yen, C. Lee, Development of battery-free neural interface and modulated control of tibialis anterior muscle via common peroneal nerve based on triboelectric nanogenerators (TENGs), Nano Energy 33 (2017) 1–11, https://doi.org/10.1016/J.NANOEN.2016.12.038.
[25] L.A. Geddes, J.D. Bourland, The strength-duration curve, IEEE Trans. Biomed. Eng. BME 32 (1985) 458–459, https://doi.org/10.1109/TBME.1985.325456.
[26] S. Jezernik, M. Morari, Energy-optimal electrical excitation of nerve fibers, IEEE Trans. Biomed. Eng. 52 (2005) 740–743, https://doi.org/10.1109/TBME.2005.844050.
[27] A.C.D. Salter, F.J.R. Richmond, G.E. Loeb, Prevention of muscle disuse atrophy by low-frequency electrical stimulation in rats, IEEE Trans. Neural Syst. Rehabil. Eng. 11 (2003) 218–226, https://doi.org/10.1109/TNSRE.2003.817674.
[28] M. Clarke Moloney, G.M. Lyons, P. Breen, P.E. Burke, P.A. Grace, Haemodynamic study examining the response of venous blood flow to electrical stimulation of the gastrocnemius muscle in patients with chronic venous disease, Eur. J. Vasc. Endovasc. Surg. 31 (2006) 300–305, https://doi.org/10.1016/J.EJVS.2005.08.003.
[29] A.A. Goddard, C.S. Pierce, K.J. McLeod, Reversal of lower limb edema by calf muscle pump stimulation, J. Cardiopulm. Rehabil. Prev. 28 (2008), https://journals.lww.com/jcrjournal/Fulltext/2008/05000/Reversal_of_Lower_Limb_Edema_by_Calf_Muscle_Pump.3.aspx.
[30] V.Y. Bogachev, O.V. Golovanova, A.N. Kuznetsov, A.O. Shekoyan, N. Bogacheva, Electromuscular Stimulation with VEINOPLUS® for the Treatment of Chronic Venous Edema, (2011).
[31] J. Ludbrook, The musculovenous pumps of the human lower limb, Am. Heart J. 71 (1966) 635–641, https://doi.org/10.1016/0002-8703(66)90313-9.
[32] J. Wang, H. Wang, N.V. Thakor, C. Lee, Self-powered direct muscle stimulation using a triboelectric nanogenerator (TENG) integrated with a flexible multiple-channel intramuscular electrode, ACS Nano 13 (2019) 3589–3599, https://doi.org/10.1021/acsnano.9b00140.
[33] L. Xu, H. Wu, G. Yao, L. Chen, X. Yang, B. Chen, X. Huang, W. Zhong, X. Chen, Z. Yin, Z.L. Wang, Giant voltage enhancement via triboelectric charge supplement channel for self-powered electroadhesion, ACS Nano 12 (2018) 10262–10271,

https://doi.org/10.1021/acsnano.8b05359.
[34] G. Cheng, Z.-H. Lin, L. Lin, Z. Du, Z.L. Wang, Pulsed nanogenerator with huge instantaneous output power density, ACS Nano 7 (2013) 7383–7391, https://doi.org/10.1021/nn403151t.
[35] Y. Zi, H. Guo, J. Wang, Z. Wen, S. Li, C. Hu, Z.L. Wang, An inductor-free auto-power-management design built-in triboelectric nanogenerators, Nano Energy 31 (2017) 302–310, https://doi.org/10.1016/J.NANOEN.2016.11.025.
[36] Y. Zi, J. Wang, S. Wang, S. Li, Z. Wen, H. Guo, Z.L. Wang, Effective energy storage from a triboelectric nanogenerator, Nat. Commun. 7 (2016) 10987 https://doi.org/10.1038/ncomms10987.
[37] C.L. Li, A. Bak, Excitability characteristics of the A- and C-fibers in a peripheral nerve, Exp. Neurol. 50 (1976) 67–79, https://doi.org/10.1016/0014-4886(76)90236-3.
[38] E.F. Evans, The frequency response and other properties of single fibres in the Guinea-pig cochlear nerve, J. Physiol. 226 (1972) 263–287, https://doi.org/10.1113/jphysiol.1972.sp009984.
[39] A. Kral, R. Hartmann, D. Mortazavi, R. Klinke, Spatial resolution of cochlear implants: the electrical field and excitation of auditory afferents, Hear. Res. 121 (1998) 11–28, https://doi.org/10.1016/S0378-5955(98)00061-6.
[40] R. Hartmann, G. Topp, R. Klinke, Discharge patterns of cat primary auditory fibers with electrical stimulation of the cochlea, Hear. Res. 13 (1984) 47–62, https://doi.org/10.1016/0378-5955(84)90094-7.
[41] P.E. Crago, P.H. Peckham, G.B. Thrope, Modulation of muscle force by recruitment during intramuscular stimulation, IEEE Trans. Biomed. Eng. BME- 27 (1980) 679–684, https://doi.org/10.1109/TBME.1980.326592.
[42] D. Popovic, L.L. Baker, G.E. Loeb, Recruitment and comfort of BION implanted electrical stimulation: implications for FES applications, IEEE Trans. Neural Syst. Rehabil. Eng. 15 (2007) 577–586, https://doi.org/10.1109/TNSRE.2007.909816.

Hao Wang. Received his B.Eng. degree in School of Optoelectronic Information from University of Electronic Science and Technology of China in 2010, and Ph.D. degree from the National University of Singapore in 2016. He is currently a Research Fellow of ECE, NUS. His research interests are focused on nanoneedle devices for transdermal drug delivery, flexible and wearable electronics, energy harvesting and electrical neural stimulations.

Jiahui Wang. Received her B.S. degree from the Department of Microelectronic at Fudan University in 2014, and Ph.D. degree from the National University of Singapore in 2019. Her research interest includes flexible electronic for biomedical applications.

Tianyiyi He. Received her B.Eng. degree from the School of Microelectronics and Solid-state Electronics at the University of Electronic Science and Technology of China (UESTC), Chengdu, China, in 2016. She is now a Ph.D student in Electrical and Computer Engineering, NUS. Her research interests focus mainly on thermoelectrics.

Dr. Zhou Li received his Ph.D. from Peking University in Department of Biomedical Engineering in 2010, and Medical Degree from Wuhan University in Medical School, 2004. He jointed School of Biological Science and Medical Engineering of Beihang University in 2010 as an associate Professor. Currently, he is a Professor in Beijing Institute of Nanoenergy and Nanosystems, CAS. His research interests include nanogenerators, in vivo energy harvester and self-powered medical devices, biosensors.

Chengkuo Lee received his Ph.D. degree in Precision engineering from The University of Tokyo in 1996. Currently, he is the director of Center for Intelligent Sensors and MEMS, and an Associate Professor in the Department of Electrical and Computer Engineering, National University of Singapore, Singapore. In 2001, he cofounded Asia Pacific Microsystems, Inc., where he was the Vice President. From 2006 to 2009, he was a Senior Member of the Technical Staff at the Institute of Microelectronics, A-STAR, Singapore. He has contributed to more than 300 international conference papers and extended abstracts and 290 peer-reviewed international journal articles.